The 8th International Supercritical CO_2 Power Cycles Symposium
February 27 – 29, 2024, San Antonio, Texas
Paper 5

Evaluation of S-CO_2 Compressor Inlet Temperature Controllers

Gihyeon Kim
Ph.D Student
Korea Advanced Institute of Science and Technology
Daejeon, Republic of Korea

Seungkyu Lee
M.S. Student
Korea Advanced Institute of Science and Technology
Daejeon, Republic of Korea

In Woo Son
Ph.D Candidate
Korea Advanced Institute of Science and Technology
Daejeon, Republic of Korea

Jeong Ik Lee
Professor
Korea Advanced Institute of Science and Technology
Daejeon, Republic of Korea

ABSTRACT

A supercritical carbon dioxide (S-CO_2) system has characteristics of being small, simple, and effective, which makes a perfect candidate for distributed power generation. Distributed power generation is locating a power generation system near where power is demanded, which allows to increase system stability, lower initial expenditures and reducing the need of long-range transmission infrastructures. However, a distributed power system has to change its operating conditions constantly to meet the frequently changing demand. Therefore, to use an S-CO_2 system as the distributed power generation system, the load-following operation of the system is needed. The load-following control strategies of S-CO_2 systems are well-known. During the load-following operation, turbine exhaust temperature, heat source power, and mass flow are all changed. Since the S-CO_2 Brayton cycle's compressor inlet properties can become close to the critical point, changes in the inlet condition have a significant impact on the compression process. Furthermore, if the compressor inlet conditions enter the liquid-vapor dome of the T-S diagram, it may cause undesirable effect. Therefore, the compressor inlet conditions must be controlled to maintain the efficiency and stability of the compressor.

This problem can be solved by controlling the precooler heat transfer rate to operate close to the design point of the compressor. However, studies and experimental verification of the S-CO_2 precooler control have not been abundant to date. Therefore, in this study, controllers based on modern control theory were designed, and the performance of the controllers was evaluated experimentally. First, system identification is performed using the experimentally verified system analysis code to obtain the transfer function and the state space of the S-CO_2 precooler system. Next, a controller based on modern control theory is designed based on the obtained state space. The designed controllers are implemented in the Autonomous Brayton Cycle test loop constructed in KAIST for the experiments of a simple recuperated S-CO_2 Brayton cycle. The performance of the controller was verified based on the operational scenario that can occur in an actual load-following operation. Finally, based on the experimental results, a design method for a precooler controller to control the compressor inlet temperature is presented.

INTRODUCTION

Supercritical carbon dioxide (S-CO_2) power systems are small, simple, and effective [1]. They are also adaptable to a variety of heat sources, including nuclear, fossil fuels, fuel cells, and concentrated solar power [2]. These characteristics make the S-CO_2 Brayton cycle an attractive next-generation power generation system and a perfect candidate for application to distributed power sources [3]. Distributed generation is a small to medium-sized power generation system that aims to generate electricity close to the demand for electricity, and has gained attraction because it can increase system reliability, lower initial investment costs, and reduce the amount of transmission infrastructure [4]. Thus, distributed generation systems should be able to produce an adequate amount of power to meet fluctuating local electricity demand. For S-CO_2 systems, load-following operation is possible using well-studied control strategies such as turbine and heat source bypass control, inventory tank control, and compressor recirculation control [5]–[8].

The properties at the compressor inlet in the S-CO_2 Brayton cycle are the closest to the critical point in the entire cycle, so small changes have a large impact on the thermodynamic properties of the fluid. Changes in compressor inlet conditions can reduce the efficiency of the system and reduce the surge margin of the compressor, which is critical to the operational safety of the system [9]. Furthermore, if the compressor inlet condition reaches the two-phase flow region, it can cause unexpected behavior [10]. Therefore, to keep the operation of the S-CO_2 system stable and efficient, the inlet condition of the S-CO_2 must be precisely controlled. The compressor inlet temperature condition changes depending on how much heat is removed by the precooler [2]; therefore, controlling the precooler operating conditions can be used to stabilize the compressor operating conditions.

The precooler in the S-CO_2 Brayton cycle removes heat from the working fluid that passed through a turbine and a recuperator and supplies the cooled fluid to the compressor. Therefore, if proper control in the precooler allows cooling to a temperature near the critical point where the compressor can operate at optimum conditions for any given CO_2 inlet condition, the S-CO_2 Brayton cycle can operate safely and efficiently, even during transients. Thus, the control goal of the precooler system is to maintain the CO_2 side precooler outlet temperature at the compressor inlet design temperature. Among the various precooler system control variables available, using the precooler's coolant flow rate as the control variable is the simplest and fastest way to control the system. Prior researches have been conducted on S-CO_2 Brayton cycle precooler control strategies for controlling the coolant flow rate [10]–[14]. However, these studies were mostly simulation-based and lacked experimental validation. In addition, the design of the controllers was based on the classical proportional-integral-derivative (PID) method.

Analogous to the S-CO_2 Brayton cycle, the organic Rankine cycle (ORC) is a thermodynamic cycle that uses alternative working fluids other than water and air [15]. The non-ideal gas characteristics make ORC an active area of control research. Accordingly, not only PID control but also controllers using reinforcement learning and modern control theory are being studied [16], [17]. For S-CO_2 precoolers, strong real gas effects are expected compared to ORCs because S-CO_2 operates very close to the critical point. Therefore, it is necessary to explore the feasibility of utilizing controllers based on various control theories for S-CO_2 Brayton cycle precoolers to maintain the compressor inlet conditions at the desired conditions. In this paper, the controllers based on optimal control theory are selected. Based on the controller based on linear quadratic (LQ) controller, several controls were designed to reduce the error and the performance of the controller was evaluated via experiments.

To design a controller based on the optimal control theory, the system dynamics must first be identified. To present a controller design methodology that can be applied in general and can be applied to the system design stage, the system dynamics are obtained from simulation results of the system transient analysis code alone rather than relying on experimental data. This is to demonstrate the possibility that starting the controller design from a simulation of the system can in fact lead to a satisfyingly performing controller for a real system, so that in the future when the controller of other S-CO_2 power systems is designed the same methodology can be applied successfully.

To evaluate the designed controllers with experiments, the Autonomous Brayton Cycle (ABC) test loop, shown in Figure 1, constructed at KAIST is utilized [18]. The ABC test loop is a simple recuperated Brayton S-CO_2 cycle experimental facility. This research facility was constructed to perform an integrated test on the simple recuperated S-CO_2 power cycle. It consists of a magnetic bearing supported turbo alternator compressor (TAC), a printed circuit heat exchanger (PCHE) type recuperator, electric cartridge type heaters, and a PCHE type precooler. The schematic diagram of ABC test loop is shown in the right side of Figure 1, and the picture of the PCHE used in the experiment is shown in Figure 2 [19].

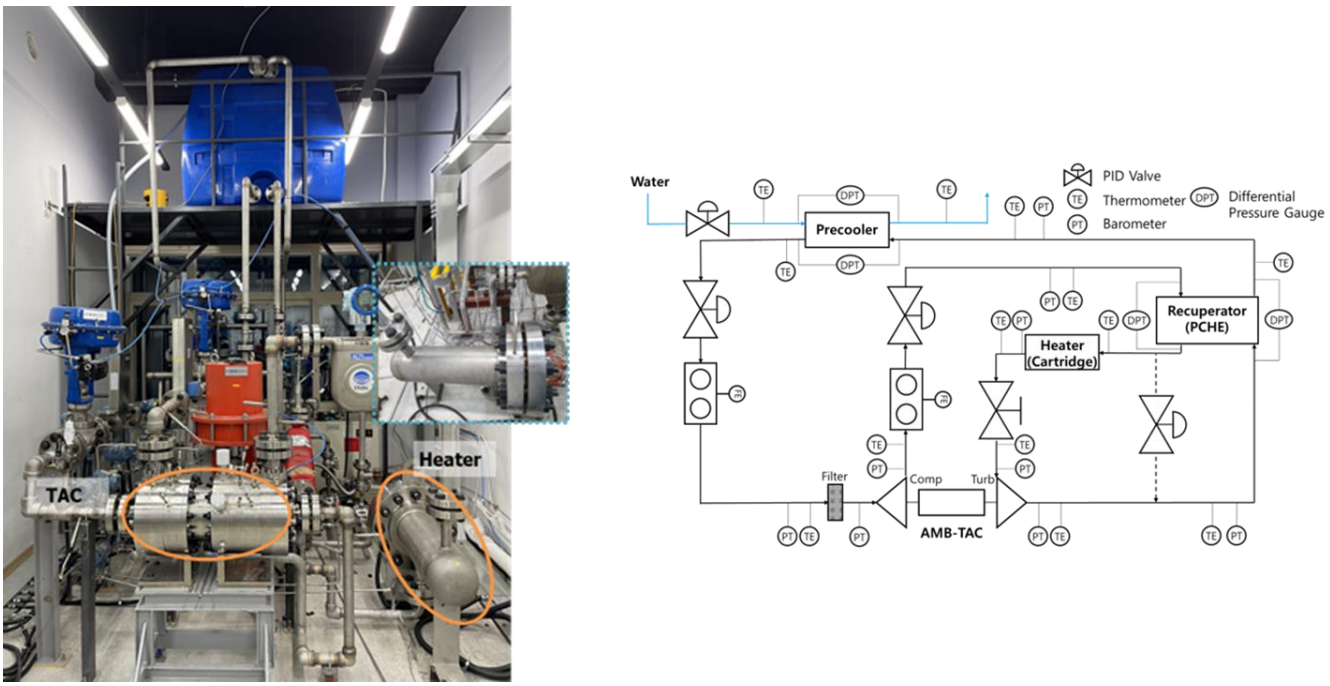

Figure 1 Front view of ABC test loop (Left), Schematic diagram of ABC test loop (Right)

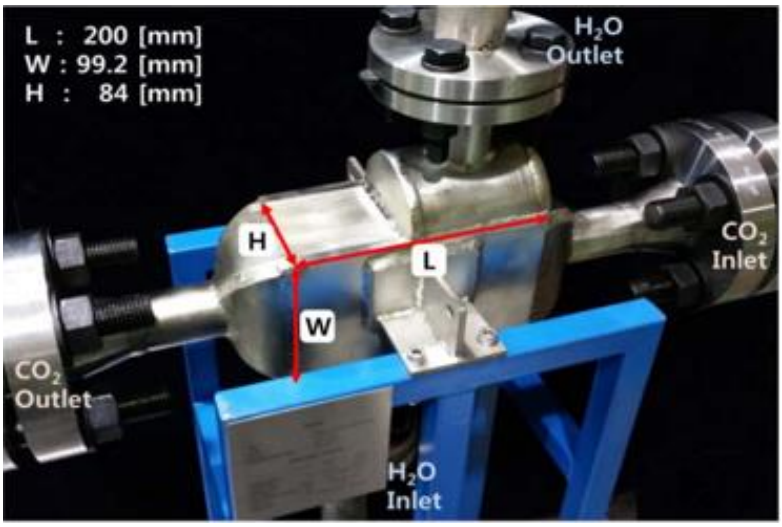

Figure 2 PCHE Type precooler used in experiment [19]

The experiments for the evaluation of the designed controller were conducted to reflect the operating conditions that may occur in actual load-following operation. The designed precooler controllers were evaluated for turbine bypass control, heater output changes, and turbomachinery speed changes, which are related to system output control. Also, since the controllers were designed based on the LQ controller from the optimal control theory, the performance of the controllers was evaluated based on the performance index as well as the size of the error.

MODELING METHODS

To design an LQ controller, the first step is to build a model based on the dynamics of the system to be controlled. For PCHE type S-CO_2 precoolers, it is well known that a model based on 1-D finite difference method (FDM) can be built, and that it is possible to calculate estimates that agree with experimental results well [19]. This model is mainly used for off-design analysis and transient analysis. However, 1-D FDM models are problematic from a control perspective. First of all, the computational time and resource requirements are overwhelming because the methodology requires recursive calculations and numerical methods. In addition, in a 1-D FDM model, temperature and pressure are calculated for each node of the heat exchanger. Since the node-specific temperature and pressure information is not needed to control the outlet temperature of the precooler, too many unnecessary calculations are performed. Therefore, a simple model is needed to estimate the amount of heat transferred from CO_2 to water in a PCHE type S-CO_2 precooler.

When analyzing a precooler system, its mechanism must be considered. The mechanism of using the water side control valve to control the CO_2 outlet temperature of the system can be divided into four steps. The first step is that the opening ratio of the water control valve is adjusted to control the system state. Second, as the valve opening ratio changes, the water mass flow rate changes. Third, as the water mass flow rate changes, the amount of heat transferred to the water changes. Finally, as the amount of heat transferred from CO_2 to water changes, the CO_2 outlet temperature changes. Therefore, the overall system diagram shown in Figure 3 can be divided into three parts as illustrated in Figure 4, which can be simplified into the block diagram depicted in Figure 5.

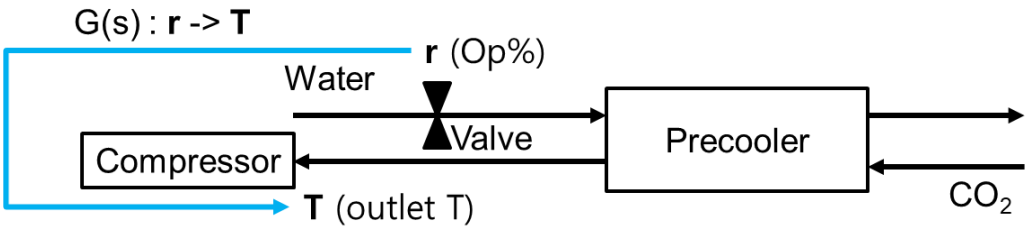

Figure 3 System diagram of precooler open loop system

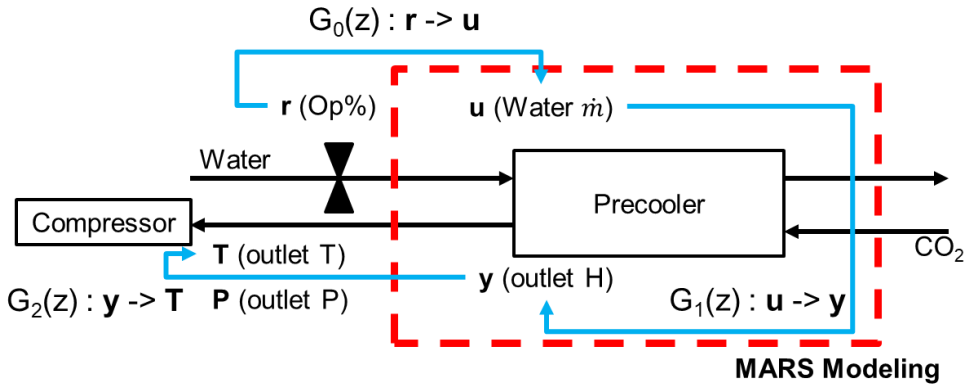

Figure 4 Modified system diagram of precooler open loop system

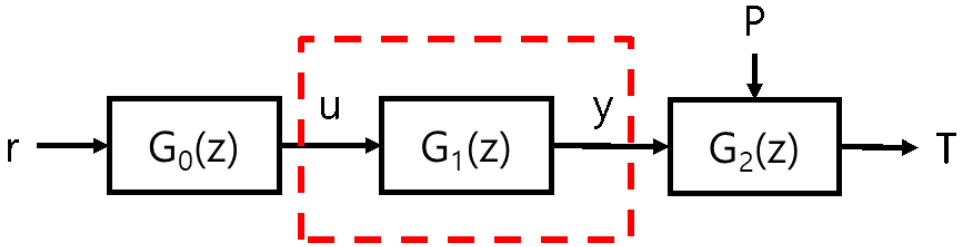

Figure 5 Modified block diagram of precooler open loop system

Figures 4 and 5 depict the three parts of the entire system. To prevent any future confusions, the system within the red dotted line is referred to as the **linearized precooler system**, and the entire system is referred to as the **precooler system**. The relationship between valve opening rate and water mass flow rate is represented by $G_0(z)$. This relationship is dependent on the valve type and can be calculated using flow coefficients and formulas provided by the valve manufacturers. $G_2(z)$ is the relationship between CO_2 outlet enthalpy and CO_2 outlet temperature. If the outlet enthalpy is known, and the outlet pressure is measured, the CO_2 outlet temperature can be calculated using a property database. In this paper, the REFPROP library was used to calculate the temperature. Therefore, it is possible to design a model of the entire precooler system by only obtaining a model for the linearized precooler system $G_1(z)$.

It is self-evident that the relationship between the precooler inlet water flow rate and the outlet CO_2 enthalpy depends on the conditions of the water and CO_2 at the precooler inlet. Therefore, the relation $G_1(z)$ of the linearized precooler system depends on the inlet conditions, which

means that continuous model modification is required when the conditions of the precooler inlet fluid deviate from the design point under load-following operating conditions. Kwon et al. presented a simple method to estimate the heat transfer when the precooler and recuperator of an S-CO_2 Brayton cycle are operating under off-design conditions [20]. The study demonstrated how the original logarithmic mean temperature difference method can be used to calculate the heat transferred from the precooler under off-design conditions. The heat transferred under off-design conditions can be obtained by multiplying the heat transfer calculated under design conditions by the linear correction factor obtained under off-design conditions. Kim et al. showed that this approach can be used for precooler system modeling, demonstrating that multiplying the system model calculated at design conditions with a lumped correction factor can predict the relationship between water flow and heat transfer in an S-CO_2 precooler [14]. Therefore, in this study, the linearized precooler system is modeled at the design point and the model is extended to the full range by utilizing the correction factor.

The Multi-dimensional Analysis of Reactor Safety (MARS) code was used for precooler system transient simulation to generalize the process and determine the transfer function between water flow and heat transfer in the precooler system at the design point. MARS is used because the PCHE model, which is needed to simulate the precooler of an S-CO_2 power system, is already implemented and validated [21]. Furthermore, since the code is heavily used by the Korean nuclear regulator for nuclear power plant licensing, the code has been well validated and verified over numerous experiments in single phase and two-phase flow regimes and heat transfer regimes, which the confidence of MARS calculation results can be regarded high.

For the PCHE precooler design conditions in the ABC test loop, CO_2 enters the precooler at 321.74 K and 7.96 MPa and exits at 308.15 K and 7.94 MPa. The temperature and pressure of the cooling water were kept at 298.15 K and 1 bar in the design conditions. Also, the temperature, pressure, and flow rate are measured every 0.5 seconds. To estimate $\mathrm{G}_1(z)$, the water flow rate was doubled in the form of a step function while keeping the inlet temperature and pressure on the CO_2 and water sides at the design conditions. In the process, the change in CO_2 enthalpy at the CO_2 outlet was simulated using the MARS code, where the output *y* of the system is the CO_2 outlet enthalpy and the control input *u* is the water flow rate. To normalize the input *u* to a unit step function, and to make the output *y* start at zero, the original input and output signals $u_{ori}(k)$ and $y_{ori}(k)$ are normalized at the *k*-th time step using equations (1) and (2). The results of the normalized MARS code simulation results are shown in Figure 6. The change in the output, $\mathrm{y}(k)$, is small compared to the input, $\mathrm{u(k)}$, because the enthalpy removed via the heat exchanger is a fraction of the total enthalpy.

$$u(k) = \frac{u_{ori}(k)}{u_{ori,min}} - 1 \quad \cdots (1)$$

$$y(k) = 1 - \frac{y_{ori}(k)}{y_{ori,max}} \quad \cdots (2)$$

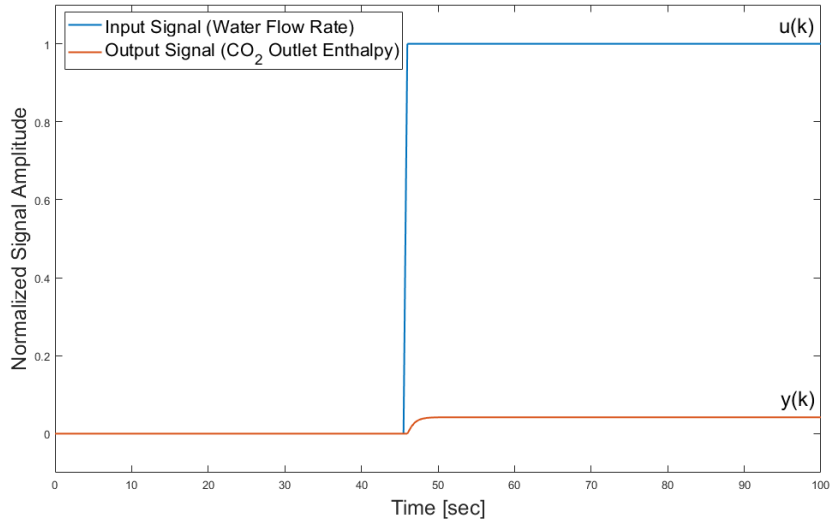

Figure 6 System response for a unit step input

For the precooler in the ABC test loop, the model $\tilde{G}_{on}(z)$ of the linearized precooler system was calculated using the least-squares method for the normalized data shown in Figure 6. Expressed in the form of a transfer function, $\tilde{G}_{on}(z)$ is given by Equation (3).

$$\frac{\mathcal{Z}\{y(k)\}}{\mathcal{Z}\{u(k)\}} = \frac{Y(z)}{U(z)} = \tilde{G}_{on}(z) = \frac{0.01989\,z\ +\ 0.004617}{z^2\ -\ 0.3074\,z\ -\ 0.1112} \cdots (3)$$

The left plot in Figure 7 shows the system response calculated with the transfer function G(z) as the blue line and the normalized result of the system response calculated with the MARS simulation as the red line. The reason the blue line is not readily visible in the graph is that the calculated value of the transfer function overlaps very well with the result from MARS. As shown in the right side of Figure 7, the maximum absolute error is 4.85×10^{-5}, which corresponds to 0.1% of the normalized value.

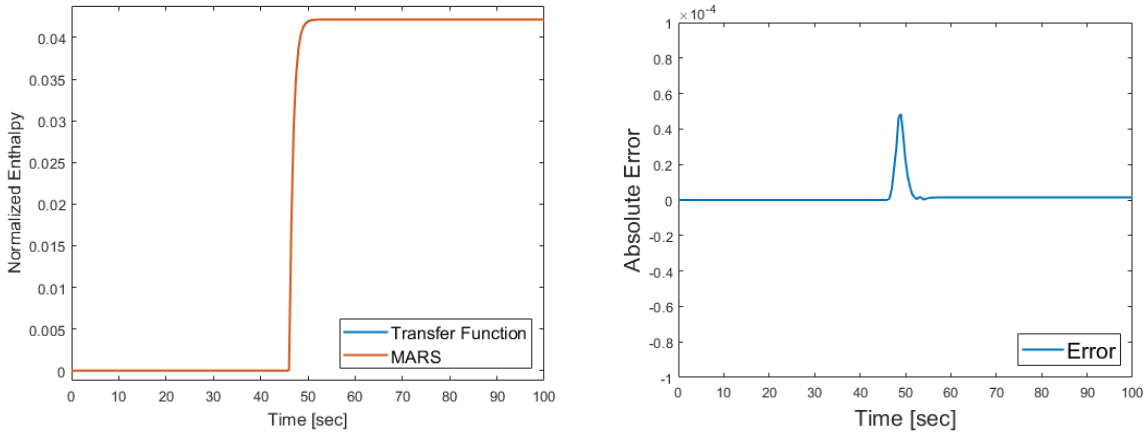

Figure 7 System response comparison for a unit step input

Therefore, it is evident that the transfer function $\tilde{G}_{on}(z)$ can be used to approximate the linearized precooler system. In this study, based on the previous works by others, the model $\tilde{G}_{on}(z)$ at the design point was extended to the off-design condition by multiplying it with a lumped correction factor C_f. The linearized precooler system model $\tilde{G}(z)$ with the correction factor C_f can be expressed as follows.

$$\tilde{G}(z) = C_f \tilde{G}_{on}(z) = C_f \frac{0.01989\,z\ +\ 0.004617}{z^2 -\ 0.3074\,z\ -\ 0.1112} \cdots (4)$$

CONTROLLER DESIGN METHODS

The linear quadratic (LQ) controller is one of the representative controllers based on the optimal control theory. The optimal control theory determines the control signals that allow a process to meet physical constraints while minimizing a certain performance criterion, thereby determining the optimal controller that minimizes a performance index [22]. The linear quadratic (LQ) controller is a well-known example of a control method that optimizes a performance index based on the state of the system and the quadratic form of the control input. For a discrete time tracking LQ controller, the performance index *J* is given by Equation (5) [23].

$$\mathrm{J} = \sum_{k=0}^{n} \left(e^T(k) Q e(k) + u^T(k) R u(k) \right) \cdots (5)$$

The performance index J in equation (5) is constructed by accumulating the sum of two terms over time at each time step. The first term, $e^T(k)Qe(k)$, is responsible for the penalty for an error at the *k*-th time step; thus, the performance index increases as the error size increases. The second term, $u^T(k)Ru(k)$, handles the penalty for inputs at the *k*-th time step. Therefore, the performance index increases as inputs become larger. The reason for introducing a penalty for the input is that the size of the input is usually related to the energy required by the controller to operate. However, the input to the precooler system, the mass flow of water, is generated by a continuously operating pump and the size of the input is regulated by a control valve. Therefore, for the precooler system, the size of the control input signal *u* is independent of the energy consumed by the controller and there is no reason to penalize the performance index. Thus, the coefficient *R* in the second term can be set to zero. Reflecting this, the performance index *J* of the precooler control system can be rewritten as in Equation (6).

$$\mathrm{J} = \sum_{k=0}^{n} e^T(k) Q e(k) \cdots (6)$$

The state feedback gain **K** that optimizes the performance index *J* in Equation (6) can be calculated by the Riccati equation, which the numerical solution is already known. In order to calculate the control inputs using the state feedback gain **K** in the LQ controller, the full state information of the system is required, thus a state observer was used to construct the controller. The block diagram of the LQ controller with the addition of a full state observer is shown in Figure 8. A block diagram of the LQ controller with the addition of a global health observer is shown in Figure 8. When applying the designed LQ controller to the precooler system, errors are expected to occur due to model uncertainties. First, there is uncertainty in the MARS modeling of the actual system. Also, there is uncertainty between the transfer function $\tilde{G}(z)$ generated from the MARS simulation and the transfer function $G_1(z)$ of the actual linearized precooler system. Finally, there is uncertainty due to the lumped correction factor C_f, which is estimated from interpolation of a

few selected off-design conditions. These model and system uncertainties contribute to the steady-state error when using an LQ controller designed for a physical system. Therefore, it is necessary to design additional control methods to eliminate this steady-state error. In this study, Disturbance OBserver (DOB), Linear Quadratic Integral (LQI), and Self-Tuning Controller were used as methods to eliminate errors in the proposed LQ controller. Each controller was designed based on the model in Equation (4). In addition, the controllers were all designed by adding additional elements to the same LQ control logic, and their performance was evaluated.

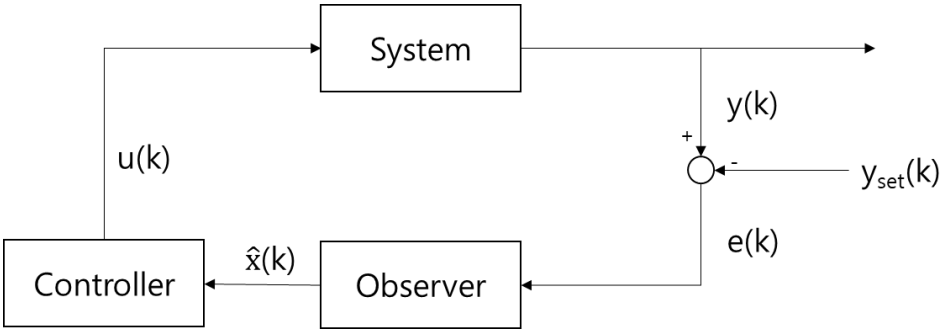

Figure 8 Block diagram of LQ controller with full-state observer

DOB aims to remove the effects of model uncertainty and external disturbances by calculating a lumped disturbance using the difference between the input-output relationship of the real system and the model [24]. By eliminating the lumped disturbance, which is calculated using the difference between the system's inputs and outputs, DOB forces the system to follow the model. This property makes DOB an effective way to remove disturbances and maintain robustness by providing stability to the model's uncertainty. For discrete time, a controller with a DOB applied can be represented by a block diagram as shown in Figure 9.

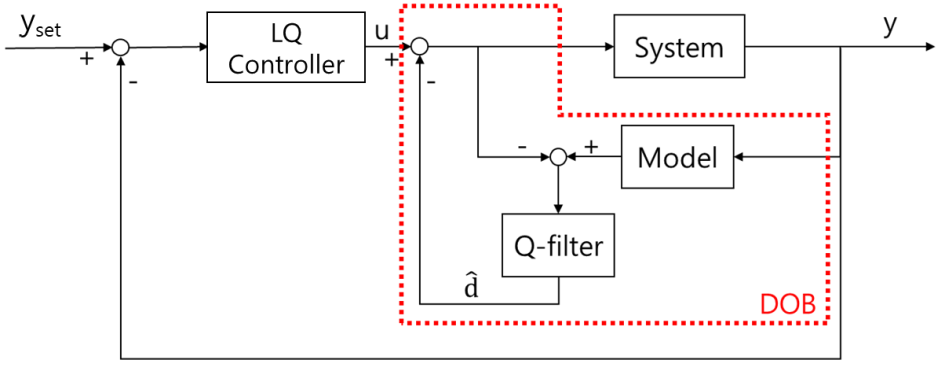

Figure 9 Block diagram of LQ controller with DOB

Since the model and controller have already been calculated, only the Q-filter needs to be selected to add the DOB to the controller. Typically, the Q-filter is chosen to be a low-pass filter with a single DC gain [25]. In this study, two low-pass filters with a single DC gain with different cutoff frequencies were used as Q-filters. The first Q-filter set the cutoff frequency much higher than the Nyquist frequency of the signal measurement, allowing all frequency components to pass through the Q-filter. The second Q-filter set the Nyquist frequency as the cutoff frequency, filtering out the higher frequency signals from the measured signal. From now on, the Q-filter with the higher cutoff frequency will be referred to as Q-filter 1 and the Q-filter with the lower cutoff frequency will be referred to as Q-filter 2. Figure 10 shows the Bode diagrams of Q-filters

1 and 2 at the measurement frequency of the experimental device. Figure 10 shows that Q-filter 2 filters the high frequency region unlike Q-filter 1.

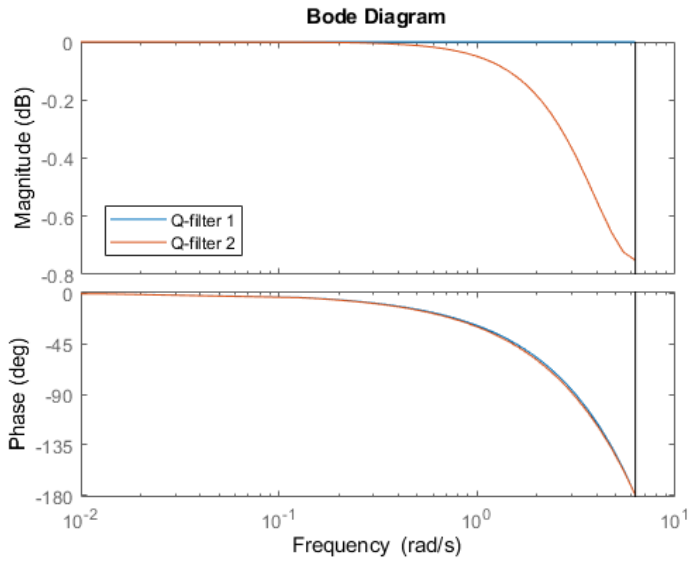

Figure 10 Bode plots of Q-filter 1 and Q-filter 2

An LQI controller is a traditional LQ controller with an integrator added. The LQI controller is designed by optimizing a performance index that includes not only the feedback gain **K** of the LQ, but also the coefficients of the integrator [26]. The integrator can be used to remove steady-state errors due to model uncertainty. This is appropriate for controlling a precooler system where steady-state error is predicted to occur due to a lumped correction factor C_f. Figure 11 shows a block diagram of the LQI controller. Like the LQ controller in Figure 8, the LQI controller obtains full-state information of the system from an observer to control it.

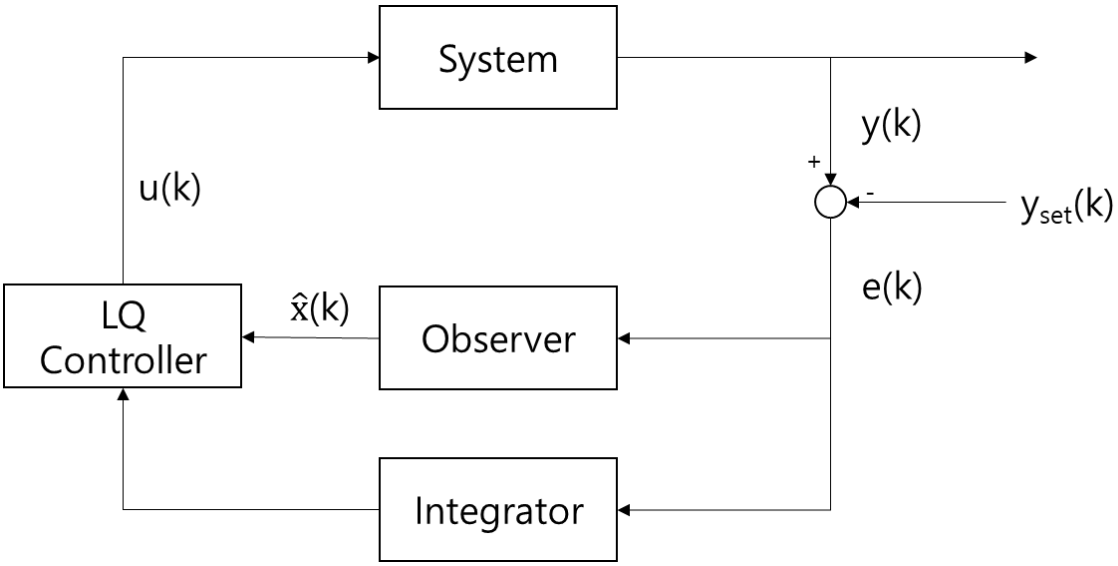

Figure 11 Block diagram of LQI controller with full-state observer

Finally, self-tuning is a method based on adaptive control that uses online information about the input signals and observed outputs of the real system to update the parameters of the controller in order to respond to changes and nonlinearities in the system over time [27]. In order to control the precooler system based on the LQ controller, it is necessary to estimate the lumped correction factor C_f. The problem is that the lumped correction factor C_f is a nonlinear and time-varying value. Therefore, a self-tuner was used to self-adjust C_f and improve the resulting error. The estimation of C_f is done in real time while the controller is operating by applying the model in Equation (4) to the input and output signals of the actual system, and the control law is updated accordingly. Figure 12 shows the block diagram of the LQ controller with a self-tuner for the lumped correction factor C_f.

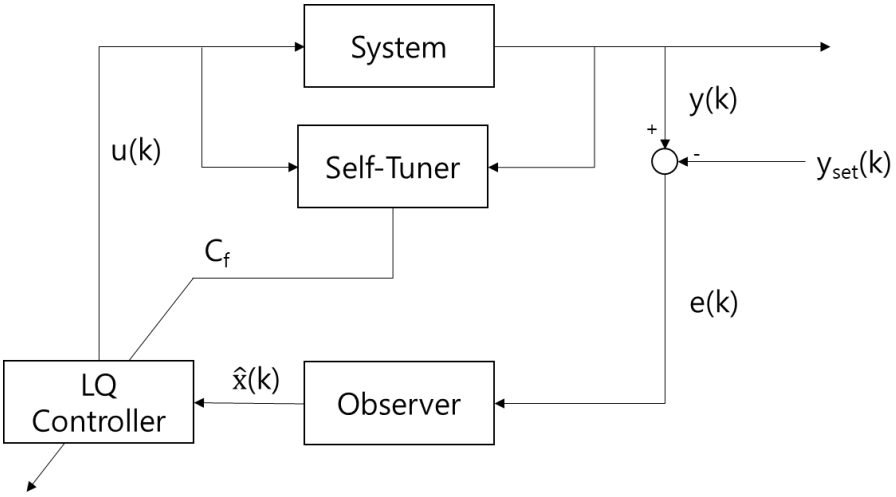

Figure 12 Block diagram of LQ controller with lumped correction factor self-tuner

EXPERIMENTAL METHODS

To regulate the inlet temperature of the compressor, an LQ controller based on the optimal control theory was designed using the system model. In addition, four more controllers were designed: two DOBs with different cutoff frequencies (i.e., Q-filter 1 and Q-filter 2), an LQI, and a self-tuning LQ controller to compensate for the modeling error expected to be mainly caused by the lumped correction factor in the LQ controller. Finally, for comparison, the PID controller simply using the Ziegler-Nichols method was designed and set as the reference [28]. All controllers were designed using only the results from the MARS simulations and did not undergo any additional tuning using experiments or simulations.

To evaluate the designed controller using the ABC test loop, an experiment was designed based on the load-following operation of the S-CO_2 system. In the ABC test loop, there are three types of disturbances associated with load-following operation: disturbances in heater power, turbine bypass, and TAC rotational speed. These three disturbances were used to test the performance of the precooler controller. If the designed controller can control the precooler to regulate the compressor inlet temperature under these three disturbance types, then the designed controller can be used for load following operation of the system.

As the compressor inlet temperature condition to be controlled, 35℃ is selected, which is the temperature of the design point. Also, the initial compressor pressure condition is selected as

78bar. The reason for setting the initial pressure higher than the design pressure of 76 bar for the compressor is to ensure a safety margin between the compressor inlet condition and the critical point in case the control fails due to controller malfunction or error. Under initial operating conditions, before any disturbance is inserted, the bypass valve is closed and the TAC and heater operate at their set values. It is noted that a fully closed bypass valve cannot be closed further. Therefore, the controller was evaluated for five scenarios (not six): increasing/decreasing heater output, opening (no closing) the turbine bypass valve, and increasing/decreasing TAC speed. In each scenario, the disturbance is removed after the system reaches steady state. Under these five scenarios, the state of the precooler CO_2 inlet changes as shown in Table 1. The parts of the ABC test loop that change for each scenario are shown in the diagram in Figure 13. The control objective of the controller is to maintain the compressor inlet temperature by adjusting the water flow rate to match the changing CO_2 inlet conditions for each scenario.

Table 1 Qualitive precooler inlet condition changes for each scenario

Scenario	Operation	Temperature	Pressure	Mass Flowrate
Scenario 1	Heater power increase	++	+	X
Scenario 2	Heater power decrease	--	-	X
Scenario 3	Bypass valve open	-	++	++
Scenario 4	TAC speed decrease	+	+	+
Scenario 5	TAC speed increase	-	-	-

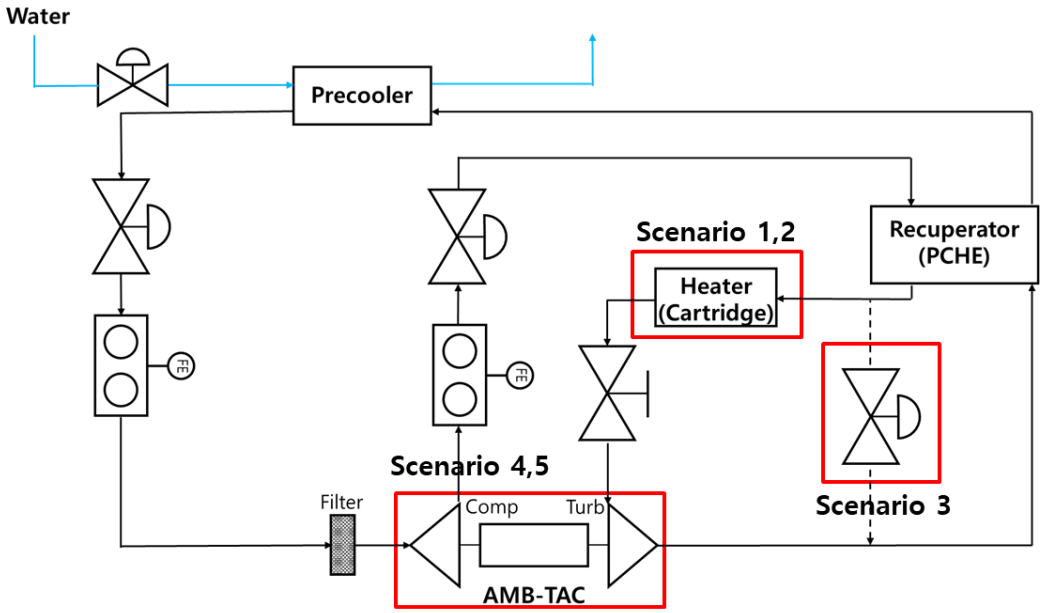

Figure 13 Disturbances in ABC test loop for controller testing

All the designed controllers were evaluated qualitatively and quantitatively using two criteria. The first criterion follows Section 3 of ASME PTC 10-1997. This performance test code presents allowable deviations and fluctuation parameters during compressor testing. According to this code, the allowable deviation of the compressor inlet temperature condition is based on absolute temperature, with an error margin of 8% and an allowable variation of 0.5%. Therefore, in this paper, the compressor inlet temperature tolerance of 0.5% is selected as the first quantitative evaluation criterion of the controller.

The second criterion is determined by the performance index. Typically, the performance index is calculated as shown in Equation (5), but as discussed earlier, the input penalty can be ignored in a precooler system, so R is set to zero as shown in Equation (6). The error $e(k)$ is the scalar difference between the setpoint temperature and the controlled compressor inlet temperature; therefore, Q is simply a value that scales the performance index, and for the simplicity of calculation, Q is set to unity. Finally, during the experiment, the amount of time each controller was subjected to the disturbance was not kept at constant. As a controller's operating time increases, the sum of squared errors accumulates, increasing the performance index *J* independent of the controller's performance. Therefore, for a quantitative comparison, the performance index was normalized by dividing it by the total operating time of the controller. The equation of J_n reflecting the two changes discussed above is presented in Equation (7). In this paper, the performance index J_n is used as the second criterion for comparing controllers, and the smaller it is, the controller performs better.

$$J_n = \frac{1}{n}\sum_{k=0}^{n}(e(k))^2 \quad \cdots (7)$$

In summary, criterion 1 evaluates the maximum error and criterion 2 evaluates how much the controller is optimized. Smaller values are preferred for both criteria. Table 2 provides a summary of the differences between the two evaluation criteria.

Table 2 Difference Between Evaluation Criteria

Name	Evaluation Parameter	Basis	Numerical Form
Criterion 1	Maximum Error	ASME PTC 10-1997 Section 3	Size of Error (%) < 0.5%
Criterion 2	Performance Index	Optimal Control Theory	$J_n = \frac{1}{n}\sum_{k=0}^{n}\left(e(k)\right)^2$

RESULTS AND DISCUSSION

Experiments were conducted on the ABC test loop using the previously presented controllers. A total of six controllers were used in the experiments: PID, LQ, LQ with DOB using Q-filters 1 and 2, LQI, and LQ with self-tuner. As mentioned earlier, all controllers were directly applied to the

ABC test loop without any additional tuning process. In other words, the controllers were designed based only on the system simulation results. Each controller was evaluated for its performance in controlling the compressor temperature inlet under a total of five disturbance scenarios. The test results for each controller are shown in Figures 14-19. The temperature at the compressor inlet is plotted in blue over time and the setpoint, which is the design temperature of the compressor, is plotted in red. The black solid lines show the maximum positive and negative error in the inlet temperature, and the dashed lines show the 0.5% error around the setpoint. The applied disturbance scenario is labeled, and the unlabeled time step represents the period during which the system stabilizes after the disturbance is removed.

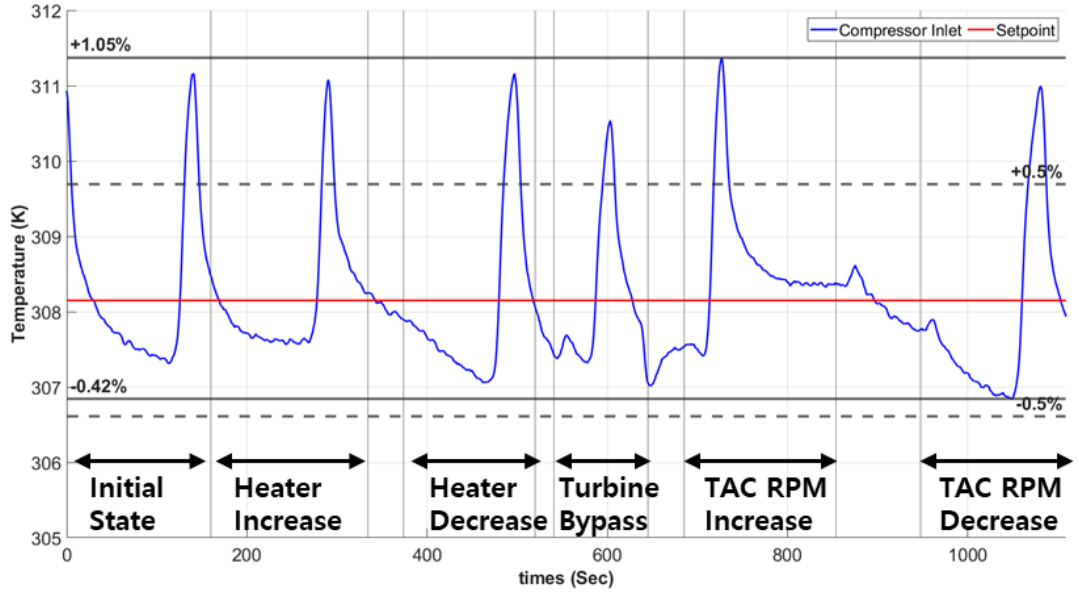

Figure 14 Control results of PID controller

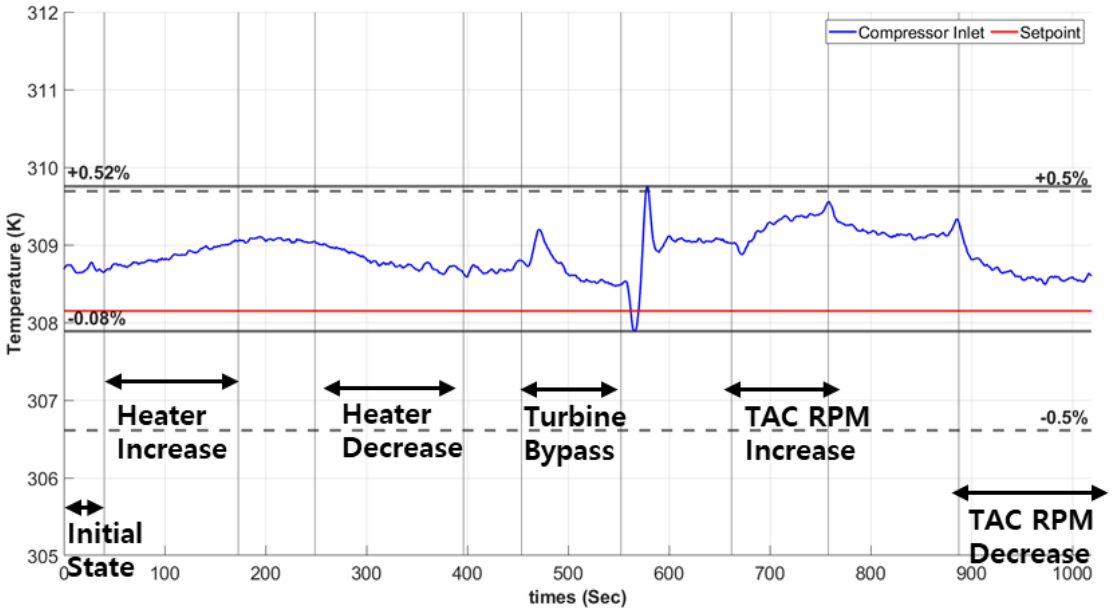

Figure 15 Control results of LQ controller

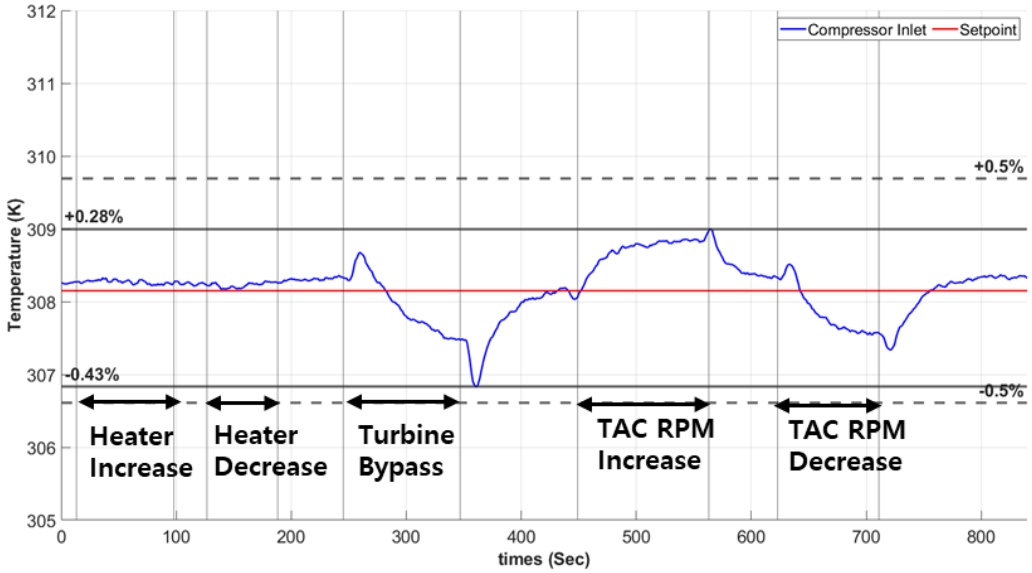

Figure 16 Control results of LQ controller with DOB Q-filter 1

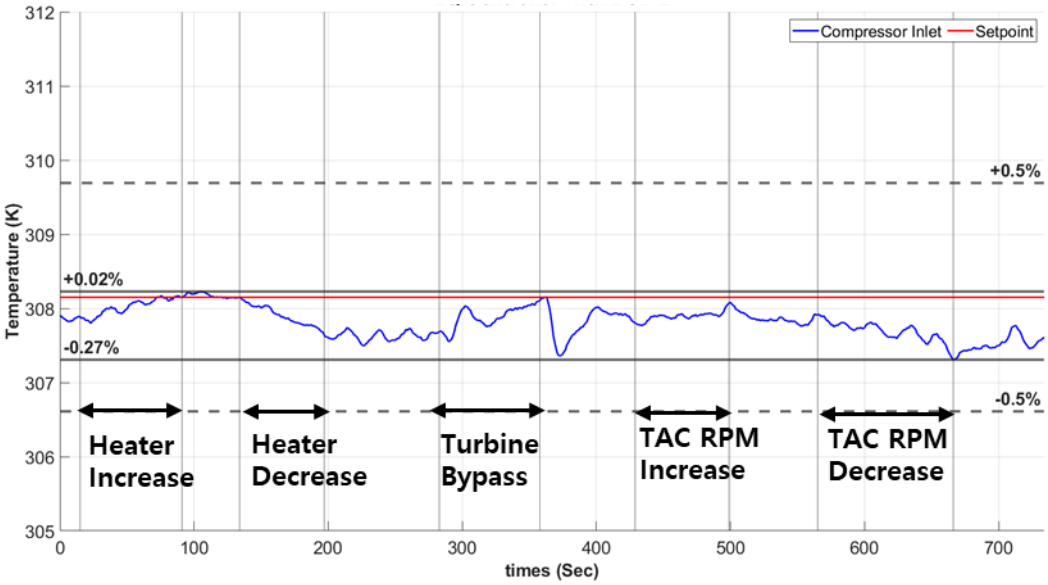

Figure 17 Control results of LQ controller with DOB Q-filter 2

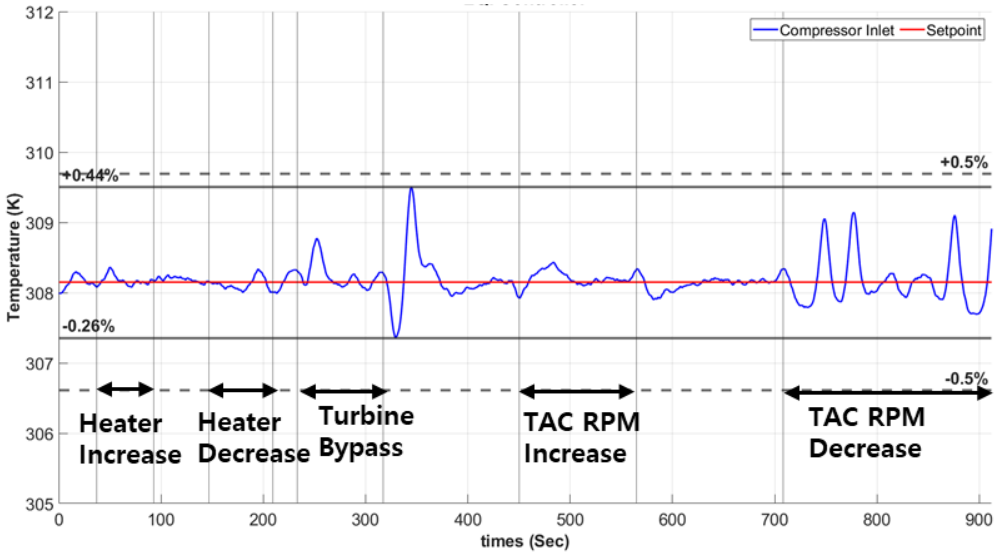

Figure 18 Control results of LQI controller

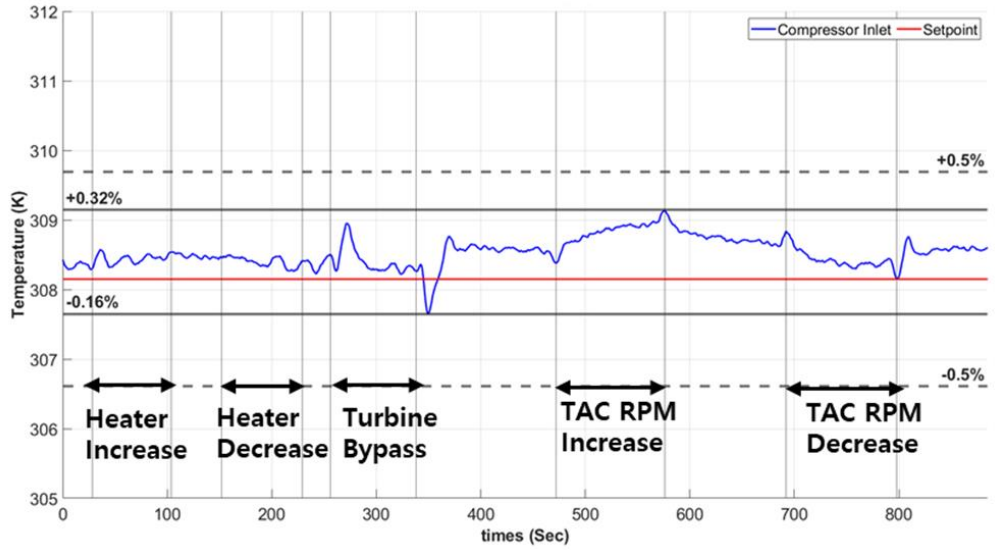

Figure 19 Control results of LQ controller with lumped correction factor self-tuner

The controllers that satisfy criterion 1 for the six controllers are LQI, LQ with DOB using Q-filters 1 and 2, and LQ with lumped correction factor self-tuner. Criterion 1 is unsatisfied for the PID and LQ controllers with the maximum error reaching 1.05% and 0.52%, respectively. From the experiment, the PID controller suffers from overshooting and oscillation, and the controller requests excessive gain, which causes it to request values beyond its control range. These factors are known limitations of the Ziegler-Nichols method, which are consistent with the experimental results. For the LQ controller, as expected, steady-state errors were detected. This occurs because the controller relies on an estimated value of the lumped correction factor C_f. It also violates criterion 1 due to the issue of speed to cope with the large flow changes that occur when the turbine bypass valve is closed.

The four controllers designed to eliminate the steady-state error of the LQ controller, LQ controller with DOB, LQI, and LQ controller with lumped correction factor self-tuner, all satisfy criterion 1. They also all show a reduction in steady-state error compared to the LQ controller in Figure 15. A qualitative analysis was performed on the four controllers. First, the LQ controller with DOB Q-filter 1 shown in Figure 16 clearly shows a reduction in steady-state error compared to the conventional LQ controller. Nevertheless, the steady-state error still exists and shows significant fluctuations when the turbine bypass valve opens and closes. Second, the LQ controller with DOB Q-filter 2 shown in Figure 17 presents a significant reduction in steady-state error compared to the LQ controller without DOB and the case with Q-filter 1. In addition, the fluctuations when the turbine bypass valve opens and closes are also significantly reduced compared to Q-filter 1. This is because the effect of the flow pulses generated by the rapid bypass fluid flow during turbine bypass operation is reduced by using a low-pass filter with the Nyquist frequency set to the cutoff frequency.

Third, the LQI controller, shown in Figure 18, also presents a reduction in steady-state error compared to the LQ controller, especially for scenarios 1 and 2. However, for scenario 5, where the rpm of the TAC decreases, the oscillations increased substantially, which is predicted to be the effect of the accumulated error due to the integrator. When the flow rate is high, the effect is not significantly observed because the accumulated error is small compared to the total flow rate. However, when the rpm of the TAC decreases in Scenario 5, the CO_2 flow rate decreases, and the effect due to the accumulated error becomes significant because even a small change in water flow rate causes a large change in the compressor inlet temperature. Finally, as shown in Figure 19, the steady-state error of the LQ controller with the lumped correction factor self-tuner is reduced compared to the LQ controller. This is the effect of reducing the inaccuracy of the model itself by using the method of calculating the lumped correction factor C_f with online updates. However, even if C_f is calculated online, the steady-state error remains. It is expected that this is caused by modeling errors other than the lumped correction factor. Therefore, it is assumed that the elimination of this steady-state error can be achieved by using a method such as DOB or LQI to eliminate modeling errors.

For the four controllers that satisfy criterion 1, the maximum error and performance index were calculated for each scenario and are shown in Tables 3 and 4, respectively. For each scenario, the cell with the minimum value was colored green and the cell with the maximum value was colored pink.

Table 3 Maximum size of error of controllers for each test scenario (Criterion 1)

Controller Type	Scenario 1	Scenario 2	Scenario 3	Scenario 4	Scenario 5	Overall
LQI	0.07%	0.06%	0.44%	0.09%	0.32%	0.44%
DOB Q-filter 1	0.06%	0.07%	0.43%	0.28%	0.26%	0.43%
DOB Q-filter 2	0.11%	0.21%	0.25%	0.13%	0.27%	0.27%
Self-Tuning LQ	0.14%	0.11%	0.26%	0.32%	0.22%	0.32%

Table 4 Performance index of controllers for each test scenario (Criteria 2)

Controller Type	Scenario 1	Scenario 2	Scenario 3	Scenario 4	Scenario 5	Overall
LQI	0.004	0.011	0.110	0.011	0.126	0.059
DOB Q-filter 1	0.014	0.016	0.235	0.277	0.182	0.153
DOB Q-filter 2	0.019	0.191	0.123	0.078	0.219	0.151
Self-Tuning LQ	0.097	0.065	0.144	0.430	0.098	0.192

Tables 3 and 4 allow to compare the performance of the controllers from the maximum size of error perspective and the optimal control perspective. From the maximum error perspective, the LQ controller with the DOB created using Q-filter 2 performed the best. From the optimal control perspective, the LQI controller performed the best. The performance was analyzed for each controller individually. First, the LQI controller achieved the minimum performance index except for Scenario 5. However, the maximum error was the largest in Scenario 3 and Scenario 5, and vibration occurred in Scenario 5. Next, for the LQ controller using DOB, comparing Q-filter 1 and Q-filter 2, the maximum error can be suppressed at the moment when the system is subjected to a disturbance by removing the high-frequency signal with an appropriate cut-off frequency. It is also the controller that kept the maximum error the smallest. However, the steady-state error remains, and the performance index is large. Finally, the LQ controller with self-tuner for the lumped correction factor minimized the maximum error and the performance index in Scenario 5. However, the steady-state error remained significant in the other scenarios, resulting in poor performance compared to the other controllers.

Therefore, the S-CO_2 system precooler controller should be selected differently depending on the operating conditions of the entire system. If the total mass flow of the system does not change rapidly within a short amount of time, and the total mass flow does not decrease from the design flow, the LQI controller should be selected. This enables optimal control by minimizing the performance index and reduces steady-state error, enabling efficient compressor operation under optimal operating conditions. On the other hand, if the total mass flow of the system changes rapidly within a short amount of time or the total mass flow decreases from the design flow, the LQI controller shows oscillation or spike in the control value due to the integrator. Therefore, in this case, it is necessary to solve the problem of accumulated error due to the integrator by using an LQ controller with DOB and self-tuner. This is a cost in performance index, but it suppresses the spike and oscillation of temperature and enables safe compressor operation.

SUMMARY AND CONCLUSIONS

The utilization of the S-CO_2 Bryton cycle for distributed generation requires to successfully meet rapidly changing loads with minimal operator action. However, without a proper control strategy, changes in system conditions due to load variations will change the conditions at the compressor inlet. If the controller is not properly designed, these changes can reduce the efficiency of the compressor and, furthermore, cause compressor surges that can lead to catastrophic failures in the system. Therefore, in this study, a method for controlling the compressor inlet temperature

conditions during such load-following operation was investigated. To precisely control the S-CO_2 compressor inlet conditions, the water cooling flow rate of the precooler was controlled.

To control the precooler cooling flow rate, the controllers based on control theory were introduced. To design the precooler control system using control theory, a model of the S-CO_2 precooler was first obtained using MARS, a well-validated system analysis code. Based on the developed system model, a controller was designed using control theory. Based on the LQ controller, four additional controllers were designed to compensate for the steady-state error caused by the inaccuracy of the lumped correction factor prediction at off-design points. All controllers were developed using only the precooler model obtained from the system simulation and did not undergo any additional tuning, in order to apply the same methodology for controlling the precooler of an arbitrary system.

All six controllers were implemented in the ABC test loop, which is an S-CO_2 simple recuperated cycle test loop. The ABC test loop was used to experimentally test the performance of the controllers in five scenarios where the rotational speed of the turbomachinery, the output of the heater, and the turbine bypass valve were manipulated. The results showed that the LQI controller performed the best in situations where the flow rate of CO_2 did not decrease or change rapidly from the design point. However, when the flow rate decreased or changed rapidly, the LQI controller showed spikes or oscillations in the control value. Under these situations, it was more beneficial to apply a DOB or self-tuner to the LQ controller.

In conclusion, controllers based on the LQ controller, designed with a well verified system code, can successfully control a physical system without the need for a further tuning process. By comparing the controllers with experiments, the optimal controller for controlling the precooler was selected. It is noted that different types of controllers are optimal depending on the characteristics of the system. LQI is optimal when the CO_2 mass flow rate fluctuates less and does not go under the design flow rate, but for environments that do not meet these conditions, it was more optimal to use an LQ controller with a DOB and a self-tuner. This conclusion allows the compressor inlet temperature controller for S-CO_2 systems to be designed in advance, even at the system design stage. The controller also allows the system to operate more efficiently with less operator intervention.

REFERENCES

[1] K. J. Kimball and E. M. Clementoni, “Supercritical carbon dioxide brayton power cycle development overview,” in *Turbo Expo: Power for Land, Sea, and Air*, American Society of Mechanical Engineers, 2012, pp. 931–940.

[2] Y. Ahn *et al.*, “Review of supercritical CO2 power cycle technology and current status of research and development,” *Nucl. Eng. Technol.*, vol. 47, no. 6, pp. 647–661, 2015.

[3] J.-Y. Ryu, Ar. Ko, S.-H. Park, and J.-P. Park, “Thermo-economic assessment of molten carbonate fuel cell hybrid system combined between individual sCO2 power cycle and district heating,” *Appl. Therm. Eng.*, vol. 169, p. 114911, 2020.

[4] F. Blaabjerg, Y. Yang, D. Yang, and X. Wang, “Distributed power-generation systems and protection,” *Proc. IEEE*, vol. 105, no. 7, pp. 1311–1331, 2017.

[5] P. Wu *et al.*, “A review of research and development of supercritical carbon dioxide Brayton cycle technology in nuclear engineering applications,” *Nucl. Eng. Des.*, vol. 368,

p. 110767, 2020.

[6] B. S. Oh *et al.*, “Safety evaluation of supercritical CO2 cooled micro modular reactor,” *Ann. Nucl. Energy*, vol. 110, pp. 1202–1216, 2017.

[7] N. Carstens, “Control strategies for supercritical carbon dioxide power conversion systems,” Massachusetts Institute of Technology, 2007.

[8] M. Marchionni, G. Bianchi, and S. A. Tassou, “Transient analysis and control of a heat to power conversion unit based on a simple regenerative supercritical CO2 Joule-Brayton cycle,” *Appl. Therm. Eng.*, vol. 183, p. 116214, 2021.

[9] Y. Jeong, “Development of correction method considering real gas effect for S-CO $ _2 $ compressor performance evaluation and operating limits,” 2023.

[10] S. A. Wright, R. F. Radel, M. E. Vernon, P. S. Pickard, and G. E. Rochau, “Operation and analysis of a supercritical CO2 Brayton cycle.,” Sandia National Laboratories (SNL), Albuquerque, NM, and Livermore, CA …, 2010.

[11] A. Heifetz and R. Vilim, “Turbine bypass, mass inventory, and mixed-mode generator power control of S-CO2 recompression cycle,” *Nucl. Technol.*, vol. 189, no. 3, pp. 268–277, 2015.

[12] B. S. Oh, J.-I. Lee, S. G. Kim, S. K. Cho, and H. Yu, “Transient analyses of S-CO2 cooled KAIST Micro Modular reactor with GAMMA+ code,” in *NUTHOS-11: The 11th International Topical Meeting on Nuclear Reactor Thermal Hydraulics, Operation and Safety (2016)*, American Nuclear Society, 2016.

[13] E. Anselmi, I. Bunce, V. Pachidis, P. Zachos, and M. Johnston, “An overview of the Rolls-Royce sCO2-test rig project at Cranfield University,” 2018.

[14] G. H. Kim and J. I. Lee, “STUDY OF PID-BASED S-CO<inf>2</inf> PRECOOLER SYSTEM CONTROL METHOD,” in *Conference Proceedings of the European sCO2 Conference*, 2023. doi: 10.17185/duepublico/77265.

[15] C. Sprouse and C. Depcik, “Review of organic Rankine cycles for internal combustion engine exhaust waste heat recovery,” *Appl. Therm. Eng.*, vol. 51, no. 1, pp. 711–722, 2013, doi: https://doi.org/10.1016/j.applthermaleng.2012.10.017.

[16] M. Imran, R. Pili, M. Usman, and F. Haglind, “Dynamic modeling and control strategies of organic Rankine cycle systems: Methods and challenges,” *Appl. Energy*, vol. 276, p. 115537, 2020.

[17] M. A. Rahmani, M. Alamir, D. Gualino, and V. Rieu, “Nonlinear dynamic model identification and MPC control of an Organic Rankine Cycle (ORC) based solar thermal power plant,” in *2015 European Control Conference (ECC)*, IEEE, 2015, pp. 2539–2546.

[18] J. Y. Baek, J. J. Lee, and J. I. Lee, “System Modeling of KAIST S-CO2 ABC Test Loop,” *Trans. Korean Nucl. Soc. Spring Meet.*, 2022.

[19] S. Baik, S. G. Kim, J. Lee, and J. I. Lee, “Study on CO2–water printed circuit heat

exchanger performance operating under various CO_2 phases for S-CO_2 power cycle application," *Appl. Therm. Eng.*, vol. 113, pp. 1536–1546, 2017.

[20] J. S. Kwon, S. J. Bae, J. Y. Heo, and J. I. Lee, "Development of accelerated PCHE off-design performance model for optimizing power system operation strategies in S-CO2 Brayton cycle," *Appl. Therm. Eng.*, vol. 159, p. 113845, 2019.

[21] J. Y. Baek, J. J. Lee, S. J. Kim, and J. I. Lee, "Improvements of MARS Code for Analyzing S-CO2 Cycle Coupled to PWR type SMR," in *Transactions of the Korean Nuclear Society Autumn Meeting*, 2019.

[22] D. E. Kirk, *Optimal Control Theory: An Introduction*. in Dover Books on Electrical Engineering Series. Dover Publications, 2004. [Online]. Available: https://books.google.co.kr/books?id=fCh2SAtWIdwC

[23] L. Weiss, "Controllability, realization and stability of discrete-time systems," *SIAM J. Control*, vol. 10, no. 2, pp. 230–251, 1972.

[24] K. Ohishi, "Torque-speed regulation of DC motor based on load torque estimation," *Proc. IEEJ IPEC, Tokyo, Japan, 1983-3*, vol. 2, pp. 1209–1216, 1983.

[25] B. K. Kim and W. K. Chung, "Advanced disturbance observer design for mechanical positioning systems," *IEEE Trans. Ind. Electron.*, vol. 50, no. 6, pp. 1207–1216, 2003.

[26] B. Porter, "Optimal control of multivariable linear systems incorporating integral feedback," *Electron. Lett.*, vol. 7, no. 8, pp. 170–172, 1971.

[27] K. J. Åström and B. Wittenmark, *Adaptive control*. Courier Corporation, 2013.

[28] J. G. Ziegler and N. B. Nichols, "Optimum settings for automatic controllers," *Trans. Am. Soc. Mech. Eng.*, vol. 64, no. 8, pp. 759–765, 1942.

ACKNOWLEDGEMENTS

This research was supported by the Challengeable Future Defense Technology Research and Development Program through the Agency For Defense Development(ADD) funded by the Defense Acquisition Program Administration(DAPA) in 2024((No.912767601)